IGI Global
PUBLISHER of TIMELY KNOWLEDGE
www.igi-global.com

Digital Charge Estimation for Piezoelectric Actuators, an Artificial Intelligence Approach

Morteza Mohammadzaheri[1,2], Hamidreza Ziaiefar[2], Mojtaba Ghodsi[3]
[1]Birmingham City University, UK, [2]Sultan Qaboos University, Oman
[3]University of Portsmouth, UK

ABSTRACT

For many piezoelectric actuators and their areas of operating, charge is proportional to the position of the actuator. Thus, for such actuators, estimation of charge is largely considered as an equivalent to position estimation. That is, a charge estimator may replace a costly and troublesome position sensor. Nevertheless, a significant portion of the excitation voltage is wasted for charge estimation. This squandered voltage, not used to deform the actuator, is called voltage drop. A class of charge estimators of piezoelectric actuators have a resistor in series with the actuator and can only work together with a digital processor. These are called digital charge estimators and have been shown to witness the smallest voltage drop compared to other charge estimators. This chapter first proposes a design guide for digital charge estimators of piezoelectric actuators to maximise the accuracy with the smallest possible voltage drop. The chapter then details the use of five different artificial intelligence (AI) techniques to tackle this design problem and assess their effectiveness through even-handed comparison.

Keywords: Piezoelectric Actuator, Charge, Voltage Drop, Precision, Artificial Neural Network, Fuzzy, Radial Basis Function, Fully Connected Cascade Network.

INTRODUCTION

Piezoelectricity, the inter-convertibility of mechanical and electrical quantities in so-called piezoelectric materials was discovered in 19th century by Curie brothers (Jayesh Minase et al., 2010). Currently, quartz and other crystals, ferroelectric polycrystalline ceramics, piezoceramics (e.g. barium titanate), and most commonly lead zirconate titanate (PZT) are used to produce piezoelectric materials (Aggrey et al., 2020; Izyumskaya et al., 2007; Jayesh Minase et al., 2010; Yang et al., 2020).

In piezoelectric materials, electrons are distributed asymmetrically in ions (Sabek et al., 2015). Therefore, mechanical force, which moves ions, provides energy to electrons, and this results in electrical voltage. In addition, electrical voltage, through pushing electrons, moves ions and generates deformation. The latter case is known as inverse piezoelectricity (Chopra, 2002). Devices, made of piezoelectric materials and deliberately produced to employ inverse piezoelectricity, are called piezoelectric actuators(Rios & Fleming, 2014). Piezoelectric actuators have applications in energy harvesting (Hou et al., 2021) , vibration control (Singh et al., 2021) and precise positioning (Flores & Rakotondrabe, 2021) including micro/nanopositioning.

Piezoelectric actuators are both the most compact and the most precise actuators in micro/nanopositioning (Mohammadzaheri & AlQallaf, 2017). Micro/nanopositioning aims at precise position control of matter at micro/nanometre scale (Mortezaa Mohammadzaheri et al., 2021), which is not necessarily equivalent to the development of micrometric scale actuators or sensors, e.g. in (Versaci et al., 2021; Xu et al., 2019). Fine machining (Hu et al., 2021), manipulation of biological cells (Deng et al., 2021), scanning probe microscopy (Szeremeta et al., 2021) and precise robotic surgery (Meinhold et al., 2020) are among applications of micro/nanopositioning with piezoelectric actuators or piezo-actuated micro/ nanopositioning .

The key task in piezo-actuated micro/nanopositioning is precise position control of (an unfixed point/surface of) the actuator (Miri et al., 2015). The origin of the position of (a point/surface on) a piezoelectric actuator is its position at relaxed state, when the actuator has not been subject to any electrical or mechanical excitation for a considerably long period of time (e.g. some minutes). That is, position of a piezoelectric actuator is its displacement from the relaxed state. Experiments have indicated that charge of a piezoelectric actuator is proportional to its position for a wide area of operating (Bazghaleh et al., 2010; M Bazghaleh et al., 2013; J. Minase et al., 2010; Yi & Veillette, 2005). Consequently, a charge estimator can replace a costly and demanding position/displacement sensor. This has been a prominent motivation for design and built of charge estimators for piezoelectric actuators (Liu et al., 2018; Mohammadzaheri & AlQallaf, 2017; Yang et al., 2017).

All existing charge estimators need electrical element(s) (e.g. resistor(s) or capacitor(s)) in series with the piezoelectric actuator. Such elements take/waste a portion of the excitation voltage (Bazghaleh et al., 2018) . This squandered voltage does not deform the actuator, and is commonly known as "voltage drop"(J. Minase et al., 2010). It has been reported that , among existing charge estimators of piezoelectric actuators, estimators with a sensing resistor witness the smallest voltage drop (M Bazghaleh et al., 2013). These estimators, unlike others, cannot be implemented without digital processors. Hence, they are broadly named "digital charge estimators" (Mohammadzaheri, Emadi, et al., 2019).Such digital charge estimators are the focus of this book chapter.

The sensing resistor of digital charge estimators often either has a fixed resistance, e.g. in (Mohsen Bazghaleh, Steven Grainger, et al., 2013; M Bazghaleh et al., 2013; Mohsen Bazghaleh, Morteza Mohammadzaheri, et al., 2013) or a few intuitively selected resistances (M Bazghaleh et al., 2013). This book chapter shows that such estimators lead to either a considerable voltage drop or a noticeable impreciseness in wide operating areas. The chapter shows that the aforementioned dilemma can be appropriately resolved, if a varying resistance is employed and the resistance is correctly found for different operating areas. Analytical approach to find the apt resistance has been shown to suffer from inherent defects (Mohammadzaheri, Emadi, et al., 2019). This book chapter, instead, employs artificial intelligence (AI) techniques to find the apt resistance for the sensing resistor.

As detailed in "Problem Statement", the chapter particularly requires AI techniques to identify a mathematical function out of experimental input-output data. Data-driven system modelling (or regression) methods based on supervised learning suit such a purpose (Sen et al., 2020). To the best of authors' knowledge, only five existing AI methods in this category are universal approximators, with verified ability for data-driven modelling: radial basis function networks, RBFNs (both exact and efficient types), neurofuzzy networks, multi-layer perceptions (MLPs), and fully connected cascade, FFC, networks. (Chen & Chen, 1995; Morteza Mohammadzaheri, Lei Chen, et al., 2012; Mohammadzaheri, Ghodsi, et al., 2018;

Park & Sandberg, 1993; Ying, 1998). All these methods are examined in this chapter to tackle the stated problem, and their performance is compared.

The parameters of employed AI models are normally identified with one of the following general approaches or a combination of them: (i) transformation of the parameter identification problem to a matrix equation and solving the matrix equation, widely used in linear modelling and support vector machines e.g. (Azimi-Pour et al., 2020) and (ii) defining an error function and minimising/optimising this function iteratively through a derivative-based optimisation method. RBFNs are often (and in this research) identified with approach (i) and MLP and FFC networks with approach (ii). A hybrid approach is commonly used to identify the parameters of neuro-fuzzy networks. Antecedent parameters are iteratively tuned with a gradient method (approach i), but at each iteration, the parameters of the consequent are identified through the method of least square of errors, based on matrix calculations, (approach ii). Detailed information on the employed AI models in this research and their parameter identification methods is presented in section "Artificial Intelligence Approach to Approximate the Sensing Resistor"

DIGITAL CHARGE ESTIMATORS OF PIEZOELECTRIC ACTUATORS

Figure 1 depicts a schematic of a digital charge estimator. V_e is the 'excitation voltage'. V_S is the voltage across the sensing resistor, R_S, or the 'sensing voltage', and f_c is the cut-off frequency of the high-pass filter in Hz. The estimator is composed of (i) the digital part, inside the computer, (ii) an analogue to digital (A/D) converter, and (iii) an analogue part including a piezoelectric actuator and a sensing resistor.

The sensing resistor, R_S, is grounded; thus, almost all the current passing through the actuator, i_P, moves along R_S. Therefore, i_P is nearly equal to the current passing R_S , i.e. i_R. In addition, as to Kirchhoff voltage law, $V_S = i_R R_S$. Hence,

$$i_P \approx i_R = \frac{V_S}{R_S}. \tag{1}$$

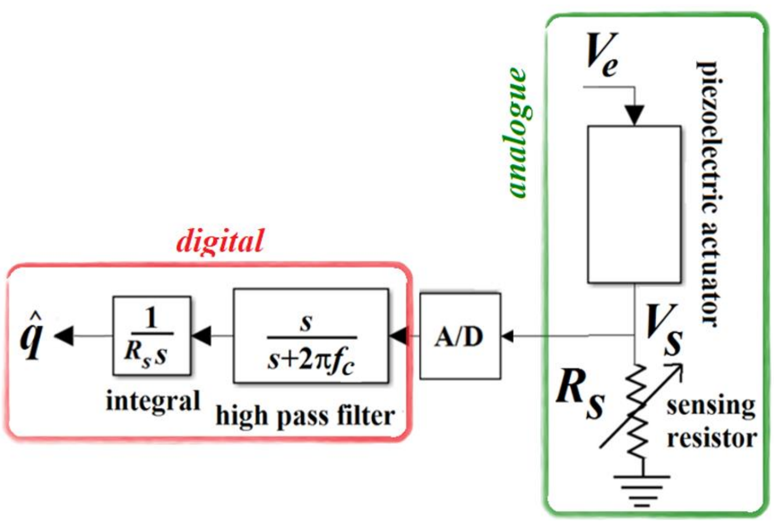

Figure1. A schematic of digital charge estimator. The estimator includes integral and high pass filter in a computer software or program (digital part), a grounded sensing resistance and the actuator (analogue part) and an A/D convertor to connect the analogue part to the digital part.

Theoretically, integral of i_P is the charge of the actuator. However, such an integration has complications. The reason is that the A/D converter, in practice, adds a miniscule offset voltage to electrons. This offset voltage besides dielectric voltage leakage of the piezoelectric actuator create a low frequency (nearly constant) tiny bias voltage, V_b. Therefore, the voltage of the current entering A/D is $V_S + V_b$, in reality. V_b is integrated together with V_S , as shown in (2), and adversely affects estimation accuracy. In summary, the estimated charge, $\hat{q}_P$, is not equal to the actual charge of the actuator, q_P:

$$\hat{q}_P = \int \frac{V_S + V_b}{R_s} dt \neq \int \frac{V_S}{R_s} dt \equiv q_P. \tag{2}$$

This discrepancy is known as drift (Mohsen Bazghaleh, Morteza Mohammadzaheri, et al., 2013). A high-pass filter, e.g. the one in Fig.1, can subdue low frequency voltage signals including V_b and accordingly prevent drift. This filter, however, suppresses low frequency components of V_S either. Consequently, digital charge estimators do not suit low frequency applications.

PROBLEM STATEMENT

Considering Fig.1, with a known A/D convertor and actuator, the main task in design/optimisation of a digital charge estimator for a piezoelectric actuator is to choose the sensing resistance, R_S. Dual rough design objectives of O1 and O2 are taken into account for this purpose:

O1- high precision

O2- low voltage drop

The A/D converter plays a critical role in the selection of R_S so as to meet the aforementioned design objectives, particularly O1. Each A/D unit has n bits resolution (e.g. 8 or 12 bits) and one or a number of range(s) for its input voltage (e.g. ±1 V, ±5 V and ±10 V). After discretisation, the input range of choice is presented by uniformly distributed 2^n digital numbers (Gray, 2006). For any given input range of the A/D converter, a wider coverage of the range by the input voltage (e.g. V_S in Fig.1) means that the input voltage is presented by more digital numbers (maximum 2^n). For example, let us assume in two digital estimators, half and full of the input range is covered by V_S. Then, V_S is presented by 2^{n-1} and 2^n digital numbers respectively. In the latter case (full coverage of the input range), each digital number refers to 50% smaller value of V_S. This simply means a higher precision. Thus, for any given resolution/input range in digital charge estimators, maximum precision is attained, if an input range of the A/D is fully covered by V_S. In other words, in order to achieve O1, R_S should be selected so as the range of V_S equals an input range of the A/D.

Voltage drop, the portion of V_e not used for actuator deformation, equals V_S. Therefore, V_S can replace voltage drop in O2, and O2 can be re-expressed as V_S should be as small as possible.

In summary, for a digital estimator with a given A/D, design objectives of O1 and O2 may result in the following design recommendations:

i- The range of V_S should be equal to an input range of the A/D.

ii- V_S should be as small as possible.

Both abovementioned recommendations, with prioritising the precision, can be merged as «Design Guide: the range of V_S should be equal to the smallest input range of the A/D».

This guide assures the maximum precision at the smallest possible voltage drop. The value(s) of R_S, in Fig. 1, meeting the aforementioned design guide are called ‘apt’ in this chapter, $\tilde{R}_S$.

Figure 2 depicts V_S for the digital estimator of Fig.1, where the actuator is a 5×5×36 mm^3 piezoelectric stack actuator (PiezoDrive, 2021) and R_S =44 Ω. The excitation voltage is a triangular function of time with the peaks 0 and 20 V and frequencies of 20 Hz and 60 Hz. The smallest input range of the A/D converter is ±0.625 V. Figure 2 shows that, with the excitation frequency of 60 Hz, the smallest input range of the A/D (±0.625 V) is almost fully covered by V_S, and the design guide is satisfied. However, with the frequency of 20 Hz, more than half of the minimum input range of the A/D is not used; that is, the design guide is not satisfied.

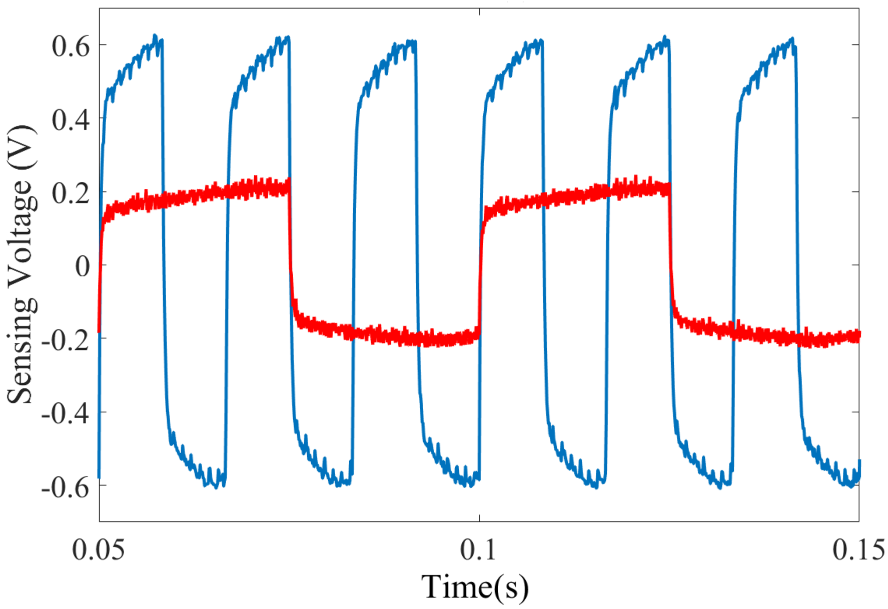

Figure 2. The range of the sensing voltage for the triangular excitation range of [0 20] V and different excitation frequencies of 20 and 60 Hz, with a 5×5× 36 mm^3 piezoelectric stack actuator and the sensing resistor of 44 Ω.

Figure 2 indicates that a digital charge estimator with a fixed R_S cannot satisfy the design guide for an extensive area of operating. While, reported digital charge estimators of piezoelectric actuators mostly use one (Mohsen Bazghaleh, Steven Grainger, et al., 2013; Mohsen Bazghaleh, Morteza Mohammadzaheri, et al., 2013) or a few intuitively selected values of R_S (M Bazghaleh et al., 2013). This chapter, alternatively, proposes an adaptive digital charge estimator with a varying R_S so as to satisfy the design guide for different operating areas. Such a digital charge estimator needs a formula (F in (3)) to approximate $\tilde{R}_S$ at various values of operating factors:

$\hat{R}_S$ =F(operating factors): range of V_S=smallest input range of the A/D (3)

where operating factors are amplitude (in V), waveform and frequency (in Hz) of the excitation voltage (V_e in Fig.1). $\hat{R}_S$ denotes an approximated value of $\tilde{R}_S$.

This chapter addresses operating areas with either sinusoidal or triangular excitation voltages, in which their use have been frequently reported in micro/nanopositioning (Morteza Mohammadzaheri, Steven Grainger, et al., 2012b; Mohammadzaheri et al., 2013; M. Mohammadzaheri et al., 2012). For either sinusoidal or triangular excitation voltage functions, operating factors are range, r, and frequency, f, of the excitation voltage:

$$\begin{cases} \hat{R}_{SS} = F_S(r, f) : r = \min(\text{input ranges of the A/D}) & \text{sinusoidal excitation} \\ \hat{R}_{ST} = F_T(r, f) : r = \min(\text{inpput ranges of the A/D}) & \text{triangualr excitation} \end{cases} \quad (4)$$

where F_S, $\hat{R}_{SS}$, F_T and $\hat{R}_{ST}$ are the equivalents of F and $\hat{R}_S$ in (3) for sinusoidal or triangular excitation voltages respectively. This chapter focuses on identification of F_S and F_T, in order to approximate $\tilde{R}_S$. Identification of F_S and F_T, with a physics-based analytical approach has been tried and shown to be inaccurate (Mohammadzaheri, Emadi, et al., 2020; Mohammadzaheri, Emadi, et al., 2019) (Mohammadzaheri; et al., 2019). This chapter employs five different artificial intelligence methods to identify F_S and F_T, compares them and interprets the findings.

EXPERIMENTAL DATA COLLECTION

Figure 3 depicts the excitation voltages used in experiments. The values of r were set to 10, 15, 20, 25, 30 and 35 V for sinusoidal excitations, and 10, 20, 30, 40 and 50 V for triangular excitations. In both cases, the values of f were 20, 30, 40, 50, 60, 70 and 80 Hz . As a result, 35 and 42 experiments were conducted for triangular and sinusoidal excitations, respectively.

The utilised piezoelectric actuator is a 5×5×36 mm^3, detailed in (PiezoDrive, 2021) . An Aetechron 7114 voltage amplifier and an Advantech PCI-1710U input/output (I/O) card were also used in experiments. The aforementioned card has A/D units with the resolution of 12 bits and five input ranges: ±10, ±5, ±2.5, ±1.25 and ±0.625 V. Moreover, MATLAB 8. 6/Simulink 8.6 software including Simulink Real-Time Desktop Toolbox 5.1 were used to generate excitation signals and observe the sensing voltages.

In each experiment, partly depicted in Fig.4, for any given excitation voltage, the sensing resistor was tuned so that the sensing voltage range became as close as possible to ±0.625 V, the smallest input range of the A/D. Such a resistance is apt ($\tilde{R}_S$) or satisfies the design guide presented in section Problem Statement. Thus, the outputs of F_S or F_T in (4) should ideally match these values of experimental $\tilde{R}_S$.

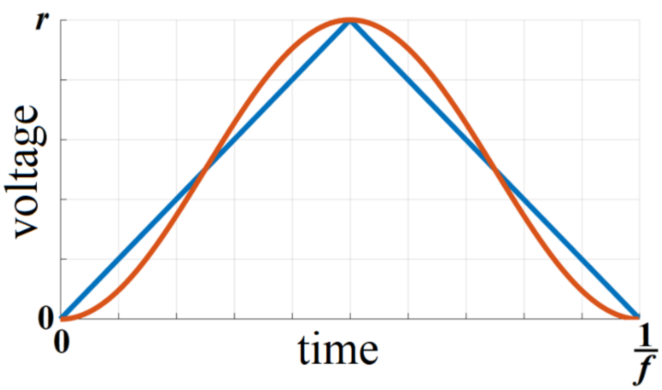

Figure 3. A cycle of excitation voltage

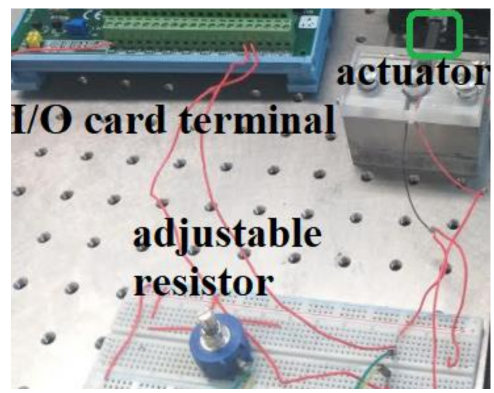

Figure 4. Parts of the experimental setup

Figure 5 shows the trend of the apt sensing resistors with change of frequency (f) for three ranges of voltage (r). It is evident that for the same f and r , triangular excitation demands a higher $\tilde{R}_S$.

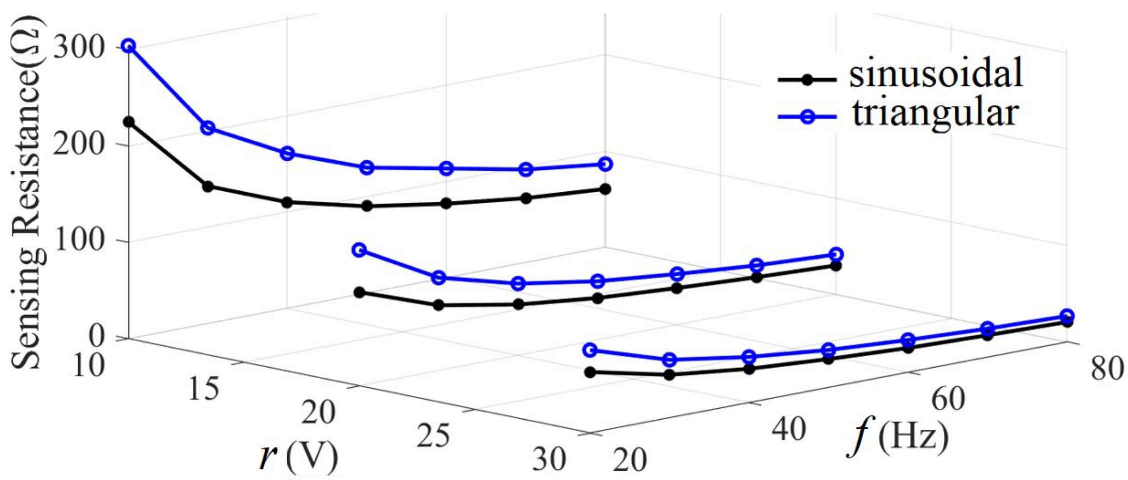

Figure 5. voltage range (r) versus frequency (f) versus the apt sensing resistance ($\tilde{R}_S$) for some of experimental data for sinusoidal and triangular excitations

ARTIFICIAL INTELLIGENCE APPROACH TO APPROXIMATE THE SENSING RESISTOR

This section reports the development of artificial intelligence models to approximate F_T and F_S in (4) with use of the collected experimental data. The employed types of models are RBFNs (both exact and efficient types), neurofuzzy networks, MLPs and FFC networks. All these models are universal approximators with proven capability to model any system when adequate data are accessible (Chen & Chen, 1995; Morteza Mohammadzaheri, Lei Chen, et al., 2012; Mohammadzaheri, Ghodsi, et al., 2018; Park & Sandberg, 1993; Ying, 1998). The models were developed through programming in MATLAB 9.4 with occasional use of commands from Neural Network Toolbox Version 11.1 and Fuzzy Logic Toolbox Version 2.3.1 of the software package.

Three series of data were employed for model developments: modelling, validation and tests data. Modelling data were used to identify the mathematical structure of the model and/or to identify the model parameters. Validation data were used to avoid overfitting. Overfitting refers to excessive focus on matching the model to the modelling data, which lessens the generality of the model (Cawley & Talbot, 2010; Mohammadzaheri et al., 2007). The test data were merely used to cross-validate the model in the end. In this chapter, hold-out or one round cross-validation was used, which simply requires the accuracy of the model with the test data to be acceptable (Lendasse et al., 2003). In this research, for each excitation function and r, seven different values of $\tilde{R}_S$ are available, one per excitation frequency (f). Amongst these seven pieces of data, five were randomly assigned to the modelling data, one to the validation data and one to the test data, as depicted in Figs.6 and 7. As to these figures, the collected experimental data are dense (Mohammadzaheri, Ziaeifar, et al., 2019; Zhang & Wang, 2016).

In all modelling methods, presented in this chapter, the aim is to minimise an error function, E, representing the discrepancy between the experimental and the approximated apt sensing resistors, $\tilde{R}_S$ and $\hat{R}_S$ (Mohammadzaheri, Emadi, et al., 2020). Mean of squared errors, defined in (5), was used as the error function in this research, as a popular option for similar problems (Mohammadzaheri, Akbarifar, et al., 2020; Mohammadzaheri, Firoozfar, et al., 2019):

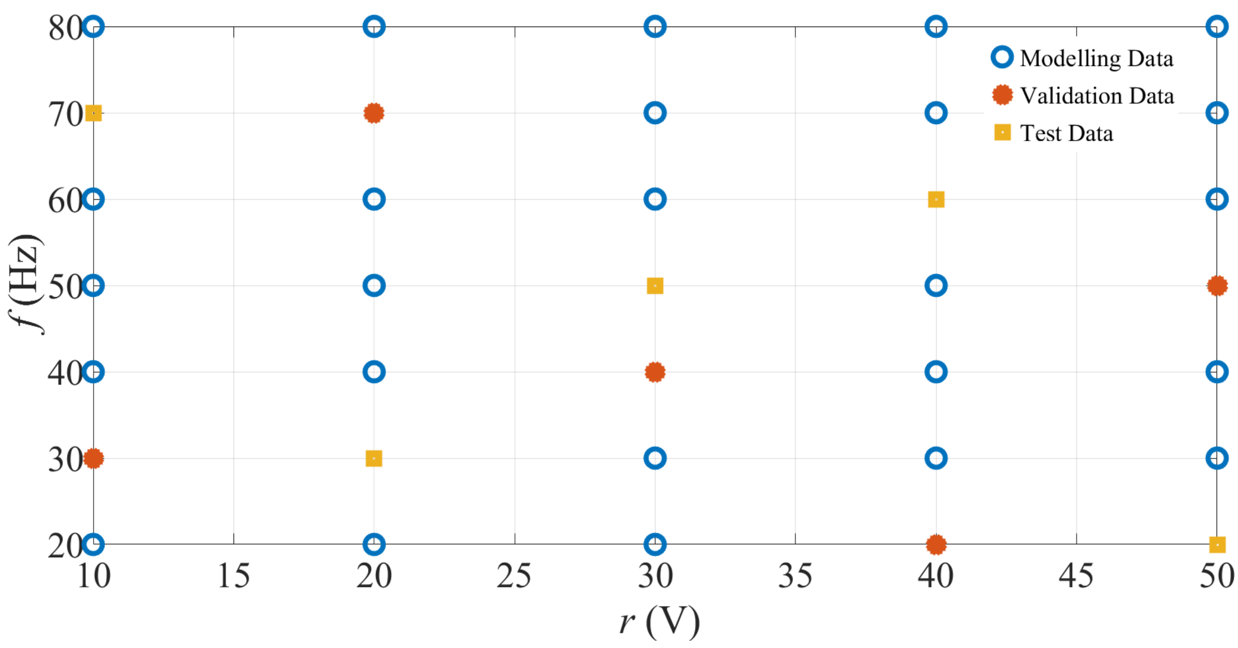

Figure 6. Voltage range (r) and frequency (f) information of modelling, validation and tests data for triangular excitation

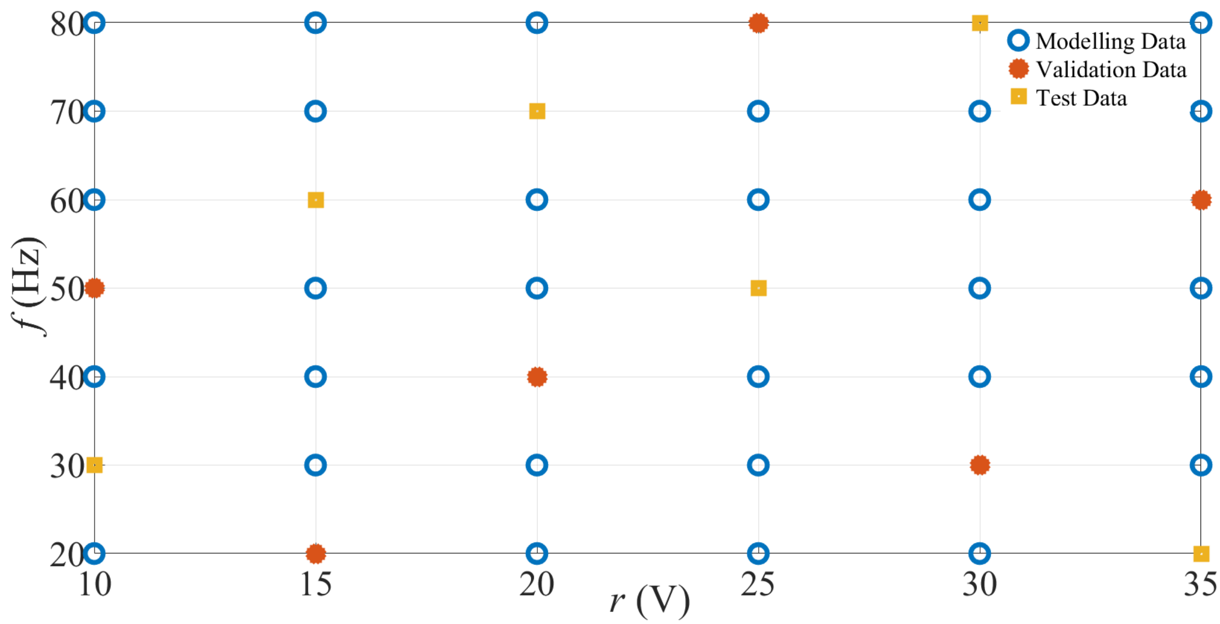

Figure 7. Voltage range (r) and frequency (f) information of modelling, validation and tests data for sinusoidal excitation

$$E = \frac{\sum_{i=1}^{n_d}\left(\hat{R}_{Si} - \tilde{R}_{Si}\right)^2}{n_d}. \tag{5}$$

where n_d is the number of samples in a data series, e.g. modelling, validation or test data. The following subsections detail different artificial intelligence techniques used in this research.

Radial Basis Function Networks (RBFNs)

An RBFN is a combination of (6) and (7). A vector of inputs, **U**, with m pairs of r and f is fed into an RBFN, and the model estimates an output vector $\hat{\mathbf{Y}}$, with up to m values of $\hat{R}_S$. Maximum value of m is the number of data sets within the modelling data, n_m (25 for triangular and 30 for sinusoidal excitation); which is also the maximum value of i and k in (6).

$$\mathbf{O}_{ik} = \exp\left(-\left(\frac{0.8326}{S}\underbrace{\sum_{j=1}^{2}\left(\mathbf{A}_{ij} - \mathbf{U}_{jk}\right)^2}_{\text{distance between input and weight arrays}}\right)^2\right). \tag{6}$$

$$\hat{\mathbf{Y}}_{1\times m} = \mathbf{B}_{1\times m} \times \mathbf{O}_{m\times m} + \mathbf{C}_{1\times m}. \tag{7}$$

where all elements of **C** are same. As to (6), the range of **O** elements is [0 1], and the condition of $\mathbf{A}_{ij}$=$\mathbf{U}_{jk}$ maximises $\mathbf{O}_{ik}$.

In RBFN modelling, arrays of **A**, **B** and **C** and the scalar of S namely 'spread' should be defined or identified. At model development stage, $\mathbf{U_M}$ and $\mathbf{Y_M}$, arrays of inputs/outputs of the modelling data were used instead of **U** and $\hat{\mathbf{Y}}$. In addition, n_m was used instead of m. Then, it was considered that $\mathbf{A}=\mathbf{U_M}^{\mathrm{T}}$ (8), where T refers to transpose. Thus, all **O** elements equalled to 1. Moreover, (9) was replaced with (7) during model development:

$$\mathbf{Y_M}_{1\times n_m} = \left[\mathbf{B}\ \ \mathbf{C}\right]_{1\times 2n_m} \begin{bmatrix} \mathbf{O} \\ \mathbf{I} \end{bmatrix}_{2n_m\times n_m} . \tag{9}$$

B and **C**, as the only unknowns of (9), were calculated. Afterwards, *S* was selected so as to minimise *E* (as defined in (5)) calculated with the validation data, also known as the validation error, *VE*. The values of 23 and 141 was opted for *S* in exact RBFNs approximating F_S *and* F_T of (4), respectively. Here is the utilised pseudo-algorithm of exact RBFN modelling to find **A**, **B**, **C** and *S* using $\mathbf{U_M}$ and $\mathbf{Y_M}$:

Step 1: Set **A**= $\mathbf{U_M}^{\mathrm{T}}$

Step 2: Set **O** $_{nm\times nm}$ =ones($n_m\times n_m$)

Step 3: Form and solve (9) with $\mathbf{Y_M}$ and **O** to find **B** and **C**

Step 4: Find *S*, with trial and error, so as to minimise the validation error of the developed RBFN

The developed exact RBFN model has $3n_m$+2 paraments (scalers or the elements of arrays) to be identified. An alternative with fewer parameters is an efficient RBFN model. In development of these models, a number of (*p*) columns of $\mathbf{U_M}$ were chosen and transposed to form **A**(Mohammadzaheri, Ghodsi, et al., 2018). Therefore, the number of **A** rows is $p \le n_m$, and (10) was replaced with (9):

$$\mathbf{Y_M}_{1\times p} = \left[\mathbf{B}\ \ \mathbf{C}\right]_{1\times 2p} \begin{bmatrix} \mathbf{O} \\ \mathbf{I} \end{bmatrix}_{2p\times p} . \tag{10}$$

RBFN modelling was started with picking a spread, *S*, and a target error, E_t. For each pair of *S* and E_t, every single column of $\mathbf{U_M}$ was transposed and considered as a single-row **A**. Then, **B** and **C** were calculated from (10), where *p*=1. The column of $\mathbf{U_M}$ resulting in the smallest modelling error, *ME*, was transposed and set as the first row of **A.** *ME* was calculated with (5) and the modelling data. Subsequently, other columns of **U** were examined to detect the column in which addition of its transpose to **A** resulted in the largest decrease of *ME***. S**uch a column was then transposed and appended to **A**. This procedure continued until *ME* reached E_t. The whole procedure to identify **A** was repeated for different pairs of *S* and E_t. The pair resulted in the lowest *VE* was opted. Based on similar research, the search space for *S* and E_t were all integers between 50 and 100 and the numbers between 1 and 10 Ω^2 with an increment of 0.1, respectively. Here is the pseudo-algorithm of efficient RBFN modelling:

Step 1: **A**=null, $\mathbf{U}_{\mathrm{rem}}$= $\mathbf{U_M}$, $\mathbf{U}_{\mathrm{opt}}$=null, *p*=1, *EX*=*VEX*=10000 (a large number), $^{\mathbf{T}}\mathbf{A}$=null (temporary weight matrix)

Step 2: Loop 1, for all values of E_t , from 0 to 10 with the increment of 0.1

Step 3: Loop 2, for all values of *S*, from 50 to 100 with the increment of 1

Step 4: Loop 3, while $EX>E_t$ *and* $p<n_m$, $p=p+1$

Step 5: Loop 4 for all values of *k*, from 1 to n_m-*p* with the increment of 1

Step 6: Add transpose of k^{th} column of $\mathbf{U}_{\mathrm{rem}}$ to **A** to form $^{\mathbf{T}}\mathbf{A}$

Step 7: Calculate **O** from (6) with $\mathbf{U}_{\mathrm{rem}}$, $^{\mathbf{T}}\mathbf{A}_{p\times \mathrm{n}}$ and *S*

Step 8: Solve (10) to find **B** and **C** ($\mathbf{Y_M}$ and **O** are available from the modelling data and step 7)

Step 9: Find the modelling error, *ME*(the model should be run more than once if $p< n_m$).

Step 10: If *ME*<*EX*, then *EX*=*ME* and $\mathbf{U}_{\mathrm{opt}}$=$\mathbf{U}_k$

Step 11: End of Loop 4

Step 12: Remove $\mathbf{U}_{\mathrm{opt}}$ from $\mathbf{U}_{\mathrm{rem}}$ and add it to **A**

Step 13: End Loop 3

Step 14: Find the validation error , VE

Step 15: If $VE<VEX$ then $VEX=VE$, $SX=S$, $E_tX=E_t$, and store **A**, **B** and **C**

Step 16: End of Loop 2

Step 17: End of Loop 1

Neurofuzzy Networks

Neurofuzzy networks, fairly similar to the ones used in (Ahmadpour Khanghashlaghi et al., 2009; Angiulli & Versaci, 2002; Lin & Chen, 2005; Mohammadzaheri, AlQallaf, et al., 2018; Morteza Mohammadzaheri, Amirhosein Amouzadeh, Mojtaba Doustmohammadi, Mohammadreza Emadi, Ehsan Jamshidi, Mojtaba Ghodsi, et al., 2021)were employed in this research. Such a neurofuzzy network, unlike RBFNs, receive single sets of inputs, i.e. a pair of r and f , and produces its associate $\hat{R}_S$. These neurofuzzy networks have n_r rules, each with two membership functions, one for r and one for f. Each input to the model, u_i, (either r of f), in j^{th} rule, goes through a Gaussian membership function of (11), which results in a membership grade,μ_{ij} (Mehrabi et al., 2017):

$$\mu_{ij} = \exp\left(-\frac{(u_i - \mathbf{D}_{ij})^2}{2\mathbf{E}_{ij}{}^2}\right). \tag{11}$$

The product of dual membership grades of a rule is considered as the weight of the rule, a real number between zero and one. The output of a rule is a linear combination of its inputs, as presented in the numerator of (12).The output of the neurofuzzy network is the weighted sum of rule outputs, similar to the model in (Mehrabi et al., 2017):

$$\hat{R}_S = \frac{\sum_{j=1}^{n_r}\left(\overbrace{\left(\sum_{i=1}^{2}\mathbf{F}_{ij}u_i + \mathbf{G}_j\right)}^{j^{th}\ rule\ output}\prod_{i=1}^{2}\mu_{ij}\right)}{\underbrace{\sum_{j=1}^{n_r}\prod_{i=1}^{2}\mu_{ij}}_{j^{th}\ rule\ weight}}. \tag{12}$$

The number of rules of the neurofuzzy model, n_r in (12) and 7 in Fig.8, as well as an initial version of the model were estimated with the modelling data through subtractive clustering algorithm. The employed subtractive algorithm is similar to the one explained in subsection 2-3 of (Morteza Mohammadzaheri, Steven Grainger, et al., 2012a). In both neurofuzzy models, for sinusoidal and triangular excitation voltages, the following parameters were used in subtractive clustering, influence range=0.5, squash factor =1.25, accept ratio=0.5 and reject ratio=0.15.

After finding n_r, the elements of **D**, **E**, **F** and **G**, as the parameters of the model, in (12), were tuned with the modelling data through an iterative algorithm. At each iteration, elements of **D** and **E** were adjusted with gradient descent error back propagation method, and the elements of **F** and **G** were found with least square of errors (LSE) method (Jang et al., 2006; Mohammadzaheri, AlQallaf, et al., 2018). The aforementioned algorithm normally leads to a continuously decreasing modelling error, ME. At every iteration. The validation error, VE, was calculated too at each iteration. Rise of VE, while ME keeps decreasing, was perceived as a sign of overfitting. In the case of such an event, aforesaid iterative algorithm was stopped.

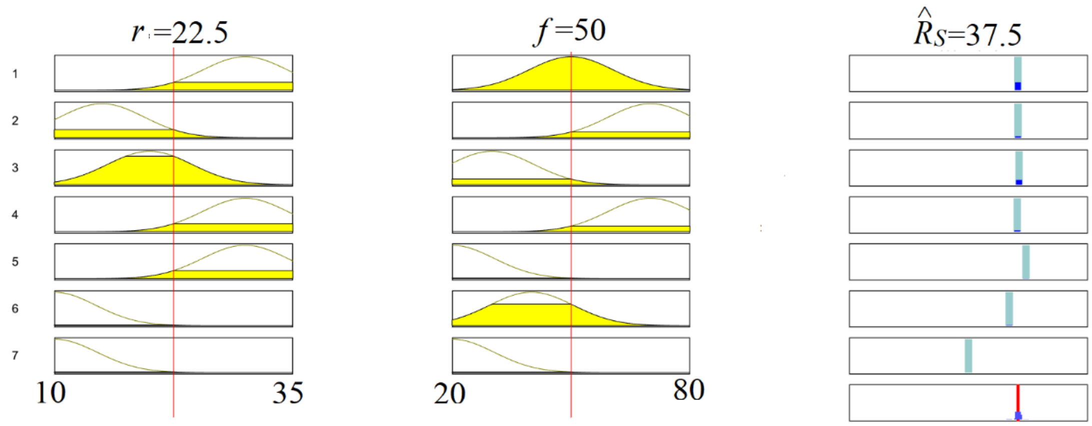

Figure 8. Rules of the neurofuzzy network for sinusoidal excitation, an approximation of F_S in (4). The values of 22.5, 50 and 37.5 show an example of pair of inputs and the estimated output.

Multi-layer Perceptrons (MLPs)

The employed MLPs, (13), receive a set of inputs, u_i |i=1 and 2 (r and f) . The MLP models of this research have one hidden layer of neurons with the activation function ϕ, presented in (14), to fit to the conditions of a universal approximator (Sifaoui et al., 2008). Kolmogorov's theorem suggests that, in MLPs with a single hidden layer, the number of neurons of the hidden layer is 2×(number of inputs)+1 (Hecht-Nielsen, 1987; Morteza Mohammadzaheri, Amirhosein Amouzadeh, Mojtaba Doustmohammadi, Mohammadreza Emadi, Ehsan Jamshidi, Mojataba Ghodsi, et al., 2021; Morteza Mohammadzaheri, Lei Chen, et al., 2012). Thus, the number of hidden layer neurons is 2×2+1=5.

$$\hat{R}_S = \sum_{j=1}^{5} \mathbf{H}_j \phi\left(\sum_{i=1}^{2} \mathbf{I}_{ij} u_i + \mathbf{J}_i \right) + \mathbf{J}_{i+1}, \tag{13}$$

$$\phi(x) = \frac{2}{1+\exp(-2x)} - 1. \tag{14}$$

The activation function of (14) is nearly a hyperbolic tangent function. This activation function has been shown to outperform other renowned activation functions such as uni-polar and bi-polar sigmoid, radial basis function (RBF) and conic section in terms of providing the MLP with a higher recognition accuracy (Karlik & Olgac, 2011; Morteza Mohammadzaheri, Amirhosein Amouzadeh, Mojtaba Doustmohammadi, Mohammadreza Emadi, Ehsan Jamshidi, Mojataba Ghodsi, et al., 2021).

Nguyen-Widrow algorithm was employed to find initial values for model parameters, **H**, **I** and **J** elements; more details of this algorithm can be found in (Mohammadzaheri et al., 2016; Nguyen & Widrow, 1990). Then, error back propagation with Levenberg-Marquardt algorithm was utilised to minimise the modelling error iteratively and to identify MLP parameters; this algorithm has been explained in (Mohammadzaheri & Chen, 2010). Parameter identification was stopped with the same procedure used for neurofuzzy networks to avoid overfitting.

As a drawback, with some initial values of MLP parameters, the employed parameter identification algorithm is trapped in so called local minima of the modelling error. This results in lack of model accuracy. Accordingly, for approximation of any model of (4) with an MLP, parameter initialisation identification was 10 times replicated with different initial parameters. The model with the smallest validation error was opted as the MLP of choice.

Fully Connected Cascade (FCC) Networks

The utilised FCC networks, in terms of mathematical structure, are MLPs with extra parameters (**N** elements) which directly connect the inputs to the output, as presented in (15) and Fig.9:

$$\hat{R}_S = \sum_{j=1}^{5} \mathbf{K}_j \phi\left(\sum_{i=1}^{2} \mathbf{L}_{ij} u_i + \mathbf{M}_i \right) + \sum_{i=1}^{2} \mathbf{N}_i u_i + \mathbf{M}_{i+1}. \tag{15}$$

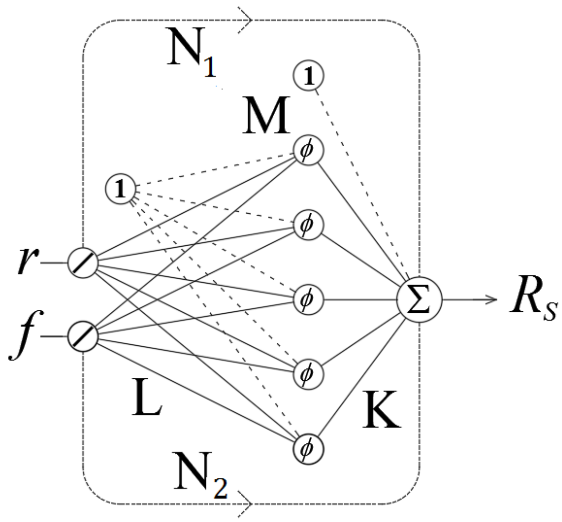

Figure 9. The schematic of an FCC used in this research. An MLP is similar to an FCC without connections which directly link the inputs to the summation function (Σ).

FCC networks use the same inputs, number of layers/neurons and activation functions as the MLPs, as well as same parameter initialisation and parameter identification algorithms. The capability of FCC networks in tackling some non-engineering benchmarks has been presented (Hunter et al., 2012), so that they have been claimed to have the most powerful architecture for system identification (Hunter et al., 2012).

RESULTS AND DISCUSSION

Figures 9 and 10 exhibit the test results, including the values of experimental $\tilde{R}_S$ and $\hat{R}_S$ approximated by different models for the tests data, never been involved in model developments reported in the previous section. For sinusoidal excitation, exact RBFN and the neurofuzzy network, each, result in an $\hat{R}_{SS}$ obviously distant from $\tilde{R}_{SS}$,shown with ∗; the second *S* in the index refers to sinusoidal, as mentioned in (4). In addition, the neurofuzzy network, both RBFNs and the FCC network produce one approximated $\hat{R}_{SS}$ recognisably distant from $\tilde{R}_{SS}$. For triangular excitations, Fig.10, all model outputs are fairly close to $\tilde{R}_{ST}$, shown with ∗; the second *T* in the index refers to triangular. However, the neurofuzzy network and both RBFNs have two values of $\hat{R}_{ST}$ detectably distant from $\tilde{R}_{ST}$; the FCC network has such an $\hat{R}_{ST}$ too.

Prior to further analysis of test results of the models, the serious risk associated with overestimation of the apt sensing resistor, $\tilde{R}_S$, needs to be clarified. From figure 1, the relationship between the excitation and the sensing voltages can be found as (16) (Mortezaa Mohammadzaheri et al., 2021):

$$\frac{V_S(s)}{V_e(s)} = \frac{R_S C_P s}{R_S C_P s + 1}. \tag{16}$$

As a result, (17) demonstrates the relationship between the magnitudes of the two voltages:

$$\frac{|V_S(\omega)|}{|V_e(\omega)|} = \frac{R_S C_P \omega}{\sqrt{R_S^{\,2} C_P^{\,2} \omega^2 + 1}}. \tag{17}$$

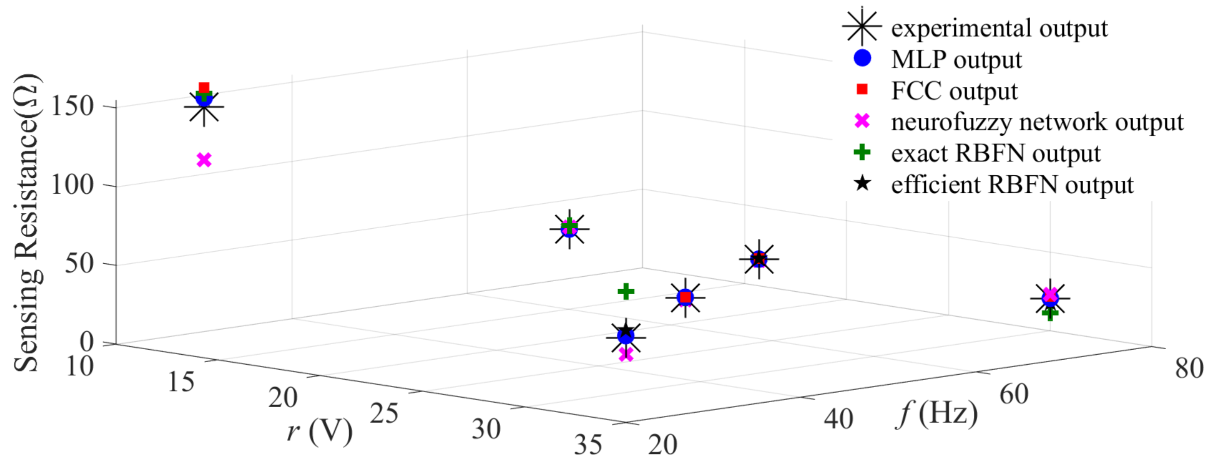

Figure 10. Test results for sinusoidal excitation

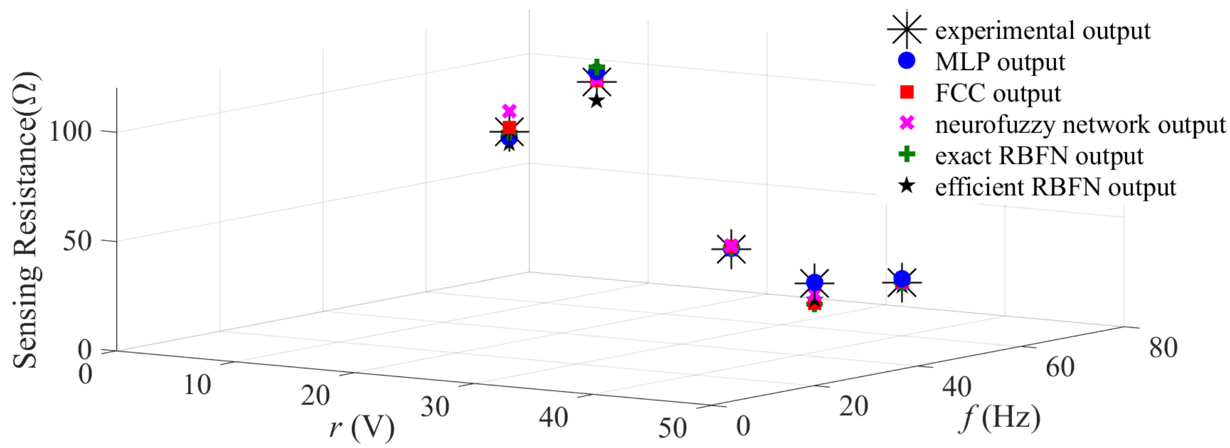

Figure 11. Test results for triangular excitation

where ω is the excitation frequency in rad/s. For a given ω, C_P and $|V_e|$, the greater the R_S, the higher $|V_S|$. Therefore, if a R_S larger than $\tilde{R}_S$ is used, $|V_S|$ exceeds its pre-defined value, i.e. 0.625 V in this research. That is, at occasions, V_S lays outside the selected input range of the A/D converter. Thus, V_S is not correctly transferred to the digital processor, or V_S is saturated. Hence, there is a great risk in overestimation of $\tilde{R}_S$, while underestimation of $\tilde{R}_S$ (i.e. too small $\hat{R}_S$) only reduces the precision, as detailed in Problem Statement section.

Let us assume error, e, and error bias, b, as
$$\begin{cases} e = \hat{R}_S - \tilde{R}_S, \\ b = \dfrac{\sum_{i=1}^{n_t} e_i}{n_t}, \end{cases} \tag{18}$$

where n_t is the number of data sets in the test data. With use of test data and considering a Gaussian distribution for e, it can be concluded that by the chance of 97%, $-3\sigma \le e\text{-}b \le 3\sigma$, (19), where σ is the standard deviation of e (Montgomery & Runger, 2017).

As a result of (19),

$$-3\sigma \le e - b \le 3\sigma \Rightarrow -3\sigma \le \hat{R}_S - \tilde{R}_S - b \le 3\sigma \Rightarrow -3\sigma - \hat{R}_S + b \le -\tilde{R}_S \le 3\sigma - \hat{R}_S + b$$

$$\Rightarrow \hat{R}_S + 3\sigma - b \ge \tilde{R}_S \ge \hat{R}_S - 3\sigma - b$$

Thus, by the chance of 97%, $\tilde{R}_S \geq \hat{R}_S - 3\sigma - b$. (20)

In order to avoid saturation of V_S, a sensing resistance of $\hat{R}_S$-3σ-b is recommended to be used, rather than $\hat{R}_S$. Therefore, a large σ results in too small values of R_S and sacrifice of precision in A/D conversion of V_S. Hence, the models with lower error standard deviation are particularly preferred.

Tables 1 and 2 provide more detailed insight into the performance of the AI models. As to both tables, MLPs clearly outperform other models and provide better results in all criteria except for the error bias. The MLPs have the smallest number of parameters amongst the models, 21, while they still fully meet the requirements of Kolmogorov's theorem. Relatively low number of parameters can play a major role in their performance, considering the fact that the modelling data could be as small as 25 data sets. For sinusoidal excitations, efficient RBFN is the second-best model with a noticeably low standard deviation. Although, disadvantageously, the number of parameters of this model is more than two times greater than the number of MLP or FCC parameters. For triangular excitations, detailed in Table 2, in terms of commonly accepted criteria of mean of squared errors and mean of absolute errors, the FCC is the second-best model after the MLP. However, the efficient RBFN is the second-best in terms of error standard deviation and maximum absolute error. In general, this research shows the claims about superiority of FCC networks, e.g. in (Hunter et al., 2012), are not valid for the problem proposed and tackled in this chapter.

Table1. Assessment of different models to estimate the apt sensing resistance with different criteria, for sinusoidal excitations

Sinusoidal Excitation	RBFN Exact	RBFN Efficient	Neurofuzzy	MLP	FCC
Mean of Absolute Errors (Ω)	8.278156	1.884255	8.516957	**1.292185**	2.808868
Max Absolute Error (Ω)	29.38565	7.889629	33.40893	**5.845352**	12.33573
Mean of Squared Errors (Ω^2)	170.7362	11.10937	207.4555	**5.979151**	26.31438
Error Standard Deviation (Ω)	11.98713	2.869653	12.58472	**2.100265**	4.292393
Error Variance (Ω^2)	143.6913	8.234907	158.3751	**4.411114**	18.42464
Error Bias (Ω)	-5.20048	-1.69542	7.005739	**-1.25221**	-2.80887
Number of Parameters	92	50	49	**21**	23

Table2. Assessment of different models to estimate the apt sensing resistance with different criteria, for triangular excitations

Triangular Excitation	RBFN Exact	RBFN Efficient	Neurofuzzy	MLP	FCC
Mean of Absolute Errors (Ω)	3.350581	4.498346	3.467672	**2.038999**	2.710431
Max Absolute Error (Ω)	9.381276	8.511782	9.401186	**4.619328**	9.02141
Mean of Squared Errors (Ω^2)	26.61291	31.34458	23.0949	**6.44773**	17.58085
Error Standard Deviation (Ω)	5.139481	3.333085	4.540334	**2.326708**	4.095632
Error Variance (Ω^2)	26.41427	11.10946	20.61463	**5.413569**	16.7742
Error Bias (Ω)	0.44569	4.498346	-1.57489	**-1.01694**	0.898133
Number of Parameters	78	50	49	**21**	23

CONCLUSION

This chapter first briefly introduced digital charge estimators of piezoelectric actuators. With given A/D converter and processor, the only adjustable element of these estimators is the resistance of their so called sensing resistor. A design guide was proposed to adjust the aforementioned resistance to maximise charge estimation accuracy with the smallest possible voltage drop. Reported experimental results showed the sensing resistance should adapt itself to the operating condition to meet the design guide.

In order to adapt the sensing resistance, a formula is needed to relate the sensing resistance to the operating conditions. The operating conditions include the relationship of excitation voltage and time (e.g. voltage is a sinusoidal and triangular function of time in this research) as well as the range and the frequency of excitation voltage. It was also shown that overestimation of the sensing resistance is seriously risky, and a method was presented to avoid it, even at the cost of some accuracy loss in charge estimation.

Accurate identification of the formula, mentioned in the previous paragraph, leads to development of highly charge/position estimators with slight voltage drop. Such estimators can replace bulky and expensive position sensors and open new horizons to nanopositioning. Analytical models have already failed to accurately identify the aforementioned formula. Alternatively, five different artificial intelligence methods were utilised to identify the aforementioned formulae: exact and efficient radial basis functions (RBFNs), neurofuzzy networks, multi-layer perceptions (MLPs) and fully connected cascade (FCC) networks. All these methods were employed even-handedly and with appropriate use of randomly chosen modelling, validation and test data, identical for all methods. MLPs show highly accurate estimation and absolute superiority over other methods. Efficient RBFN and FCC are the second-best models for different excitations/criteria. Neurofuzzy network and exact RBFN show occasional significant inaccuracy (>20Ω) in test. In summary, the results support that the MLP is a reliable option to estimate the sensing resistance and to design/optimise digital charge estimators.

REFERENCES

Aggrey, P., Salimon, A., & Korsunsky, A. (2020). Diatomite inspired nanostructured quartz as a piezoelectric material. *Limnology and Freshwater Biology*, 828-829.

Ahmadpour Khanghashlaghi, M., Yue, W. L., & Mohammadzaheri, M. (2009). *Neuro-fuzzy modelling of workders trip production* The 32nd Austalasian Transport Research Forum, Auckland, NewZealnd

Angiulli, G., & Versaci, M. (2002). A Neuro-Fuzzy Network for the design of circular and triangular equilateral microstrip antennas. *International Journal of Infrared Millimeter Waves*, *23*(10), 1513-1520.

Azimi-Pour, M., Eskandari-Naddaf, H., & Pakzad, A. (2020). Linear and non-linear SVM prediction for fresh properties and compressive strength of high volume fly ash self-compacting concrete. *Construction and Building Materials*, *230*, 117021.

Bazghaleh, M., Grainger, S., Cazzolato, B., & Lu, T.-f. (2010, December). *An innovative digital charge amplifier to reduce hysteresis in piezoelectric actuators* Australian Robotics and Automation Association (ACRA), Brisbane, Australia.

Bazghaleh, M., Grainger, S., Mohammadzaheri, M., Cazzolato, B., & Lu, T.-F. (2013). A novel digital charge-based displacement estimator for sensorless control of a grounded-load piezoelectric tube actuator. *Sensors and Actuators A: Physical*, *198*, 91-98. https://doi.org/10.1016/j.sna.2013.04.021

Bazghaleh, M., Grainger, S., Mohammadzaheri, M., Cazzolato, B., & Lu, T. (2013). A digital charge amplifier for hysteresis elimination in piezoelectric actuators. *Smart Materials and Structures*, *22*(7), 075016.

Bazghaleh, M., Grainger, S., Mohammadzaheri, M. J. J. o. I. M. S., & Structures. (2018). A review of charge methods for driving piezoelectric actuators. *Journal of Intelligent Material Systems and Structures*, *29*(10), 2096-2104.

Bazghaleh, M., Mohammadzaheri, M., Grainger, S., Cazzolato, B., & Lu, T. F. (2013). A new hybrid method for sensorless control of piezoelectric actuators. *Sensors and Actuators A: Physical*, *194*, 25-30.

Cawley, G. C., & Talbot, N. L. (2010). On over-fitting in model selection and subsequent selection bias in performance evaluation. *Journal of Machine Learning Research*, *11*(Jul), 2079-2107.

Chen, T. P., & Chen, H. (1995). Approximation capability to functions of several variables, nonlinear functionals, and operators by radial basis function neural networks. *IEEE Transactions on Neural Networks*, *6*(4), 904-910. <Go to ISI>://A1995RF58200008

Chopra, I. (2002). Review of state of art of smart structures and integrated systems. *Aiaa Journal*, *40*(11), 2145-2187. https://doi.org/10.2514/2.1561

Deng, J., Liu, S., Liu, Y., Wang, L., Gao, X., & Li, K. (2021). A 2-DOF Needle Insertion Device Using Inertial Piezoelectric Actuator. *IEEE Transactions on Industrial Electronics*.

Flores, G., & Rakotondrabe, M. (2021). Robust nonlinear control for a piezoelectric actuator in a robotic hand using only position measurements. *IEEE Control Systems Letters*.

Gray, N. (2006). ABCs of ADCs. In N. Semiconductor (Ed.).

Hecht-Nielsen, R. (1987). Kolmogorov's mapping neural network existence theorem. Proceedings of the international conference on Neural Networks,

Hou, W., Zheng, Y., Guo, W., & Pengcheng, G. (2021). Piezoelectric vibration energy harvesting for rail transit bridge with steel-spring floating slab track system. *Journal of Cleaner Production*, *291*, 125283.

Hu, C., Shi, Y., & Liu, F. (2021). Research on Precision Blanking Process Design of Micro Gear Based on Piezoelectric Actuator. *Micromachines*, *12*(2), 200.

Hunter, D., Yu, H., Pukish III, M. S., Kolbusz, J., & Wilamowski, B. M. (2012). Selection of proper neural network sizes and architectures—A comparative study. *IEEE Transactions on Industrial Informatics*, *8*(2), 228-240.

Izyumskaya, N., Alivov, Y., Cho, S. J., Morkoc, H., Lee, H., & Kang, Y. S. (2007). Processing, structure, properties, and applications of PZT thin films. *Critical Reviews in Solid State and Materials Sciences*, *32*(3-4), 111-202. https://doi.org/10.1080/10408430701707347

Jang, J. R., Sun, C., & Mizutani, E. (2006). *Neuro-Fuzzy and Soft Computing*. Prentice-Hall of India.

Karlik, B., & Olgac, A. V. (2011). Performance analysis of various activation functions in generalized MLP architectures of neural networks. *International Journal of Artificial Intelligence and Expert Systems*, *1*(4), 111-122.

Lendasse, A., Wertz, V., & Verleysen, M. (2003). Model selection with cross-validations and bootstraps—application to time series prediction with RBFN models. *Artificial Neural Networks and Neural Information Processing—ICANN/ICONIP 2003*, 174-174.

Lin, C.-J., & Chen, C.-H. (2005). Identification and prediction using recurrent compensatory neuro-fuzzy systems. *Fuzzy Sets and Systems*, *150*(2), 307-330.

Liu, S.-T., Yen, J.-Y., & Wang, F.-C. (2018). Compensation for the Residual Error of the Voltage Drive of the Charge Control of a Piezoelectric Actuator. *Journal of Dynamic Systems, Measurement, and Control*, *140*(7), 1-9.

Mehrabi, D., Mohammadzaheri, M., Firoozfar, A., & Emadi, M. (2017). A fuzzy virtual temperature sensor for an irradiative enclosure. *Journal of Mechanical Science and Technology*, *31*(10), 4989-4994.

Meinhold, W., Martinez, D. E., Oshinski, J., Hu, A.-P., & Ueda, J. (2020). A direct drive parallel plane piezoelectric needle positioning robot for MRI guided intraspinal injection. *IEEE Transactions on Biomedical Engineering*, *68*(3), 807-814.

Minase, J., Lu, T.-F., Cazzolato, B., & Grainger, S. (2010). A review, supported by experimental results, of voltage, charge and capacitor insertion method for driving piezoelectric actuators. *Precision Engineering*, *34*(4), 692-700.

Minase, J., Lu, T. F., Cazzolato, B., & Grainger, S. (2010). A review, supported by experimental results, of voltage, charge and capacitor insertion method for driving piezoelectric actuators. *Precision Engineering*, *34*(4), 692-700.

Miri, N., Mohammadzaheri, M., & Chen, L. (2015). An enhanced physics-based model to estimate the displacement of piezoelectric actuators. *Journal of Intelligent Material Systems and Structures*, *26*(11), 1442-1451.

Mohammadzaheri, M., Akbarifar, A., Ghodsi, M., Bahadur, I., AlJahwari, F., & Al-Amri, B. (2020). Health Monitoring of Welded Pipelines with Mechanical Waves and Fuzzy Inference Systems. International Gas Union Research Conference, Muscat,Oman,

Mohammadzaheri, M., & AlQallaf, A. (2017). Nanopositioning systems with piezoelectric actuators, current state and future perspective. *Science of Advanced Materials*, *9*(7), 1071-1080.

Mohammadzaheri, M., AlQallaf, A., Ghodsi, M., & Ziaiefar, H. (2018). Development of a Fuzzy Model to Estimate the Head of Gaseous Petroleum Fluids Driven by Electrical Submersible Pumps. *Fuzzy Information and Engineering*, *10*(1), 99-106.

Mohammadzaheri, M., AlSulti, S., Ghodsi, M., Bahadur, I., & Emadi, M. (2021). Assessment of capacitor-based charge estimators for piezoelectric actuators. 2021 IEEE International Conference on Mechatronics (ICM),

Mohammadzaheri, M., Amouzadeh, A., Doustmohammadi, M., Emadi, M., Jamshidi, E., Ghodsi, M., & Soltani, P. (2021). Fuzzy Analysis of Resonance Frequencies for Structural Inspection of an Engine Cylinder Block. *Fuzzy Information and Engineering*, 1-11. https://www.tandfonline.com/doi/pdf/10.1080/16168658.2021.1908819

Mohammadzaheri, M., Amouzadeh, A., Doustmohammadi, M., Emadi, M., Jamshidi, E., Ghodsi, M., . . . Engineering, M. (2021). Fault Diagnosis of an Automobile Cylinder Block with Neural Process of Modal Information. *21*(2), 1-8.

Mohammadzaheri, M., & Chen, L. (2010). Intelligent predictive control of a model helicopter's yaw angle. *Asian Journal of Control*, *12*(6), 667-679.

Mohammadzaheri, M., Chen, L., & Grainger, S. (2012). A critical review of the most popular types of neuro control. *Asian Journal of Control*, *16*(1), 1-11.

Mohammadzaheri, M., Emadi, M., Ghodsi, M., Bahadur, I. M., Zarog, M., Saleem, A. J. I. J. o. A. I., & Learning, M. (2020). Development of a Charge Estimator for Piezoelectric Actuators: A Radial Basis Function Approach. *International Journal of Artificial Intelligence and Machine Learning*, *10*(1), 31-44.

Mohammadzaheri, M., Emadi, M., Ghodsi, M., Jamshidi, E., Bahadur, I., Saleem, A., & Zarog, M. (2019). A variable-resistance digital charge estimator for piezoelectric actuators: An alternative to maximise accuracy and curb voltage drop. *Journal of Intelligent Material Systems and Structures*, *30*(11), 1699-1705.

Mohammadzaheri, M., Firoozfar, A., Mehrabi, D., Emadi, M., & Alqallaf, A. (2019). Temperature Estimation for a Point of an Infrared Dryer Using Temperature of

Neighbouring Points: An Artificial Neural Network Approach. *Journal of Engineering Research*, *7*(4).
Mohammadzaheri, M., Ghodsi, M., & AlQallaf, A. (2018). Estimate of the Head Produced by Electrical Submersible Pumps on Gaseous Petroleum Fluids, a Radial Basis Function Network Approach. *International Journal of Artificial Intelligence Applications*, *9*(1).
Mohammadzaheri, M., Grainger, S., & Bazghaleh, M. (2012a). Fuzzy modeling of a piezoelectric actuator. *International Journal of Precision Engineering and Manufacturing*, *13*(5), 663-670.
Mohammadzaheri, M., Grainger, S., & Bazghaleh, M. (2012b). Fuzzy Modeling of a Piezoelectric Actuator. *International Journal of Precission Engineering and Manufacturing*, *13*(5), 663-670.
Mohammadzaheri, M., Grainger, S., & Bazghaleh, M. (2013). A system identification approach to the characterization and control of a piezoelectric tube actuator. *Smart Materials and Structures*, *22*(10), 105022.
Mohammadzaheri, M., Grainger, S., Bazghaleh, M., & Yaghmaee, P. (2012, 2012). Intelligent modeling of a piezoelectric tube actuator. International Symposium on Innovations in Intelligent Systems and Applications (INISTA), Trabzon, Turkey.
Mohammadzaheri, M., Mirsepahi, A., Asef-afshar, O., & Koohi, H. (2007). Neuro-fuzzy modeling of superheating system of a steam power plant. *Applied Math. Sci*, *1*, 2091-2099.
Mohammadzaheri, M., Tafreshi, R., Khan, Z., Franchek, M., & Grigoriadis, K. (2016). An intelligent approach to optimize multiphase subsea oil fields lifted by electrical submersible pumps. *Journal of Computational Science*, *15*, 50-59.
Mohammadzaheri, M., Ziaeifar, H., Bahadur, I., Zarog, M., Emadi, M., & Ghodsi, M. (2019). Data-driven Modelling of Engineering Systems with Small Data, a Comparative Study of Artificial Intelligence Techniques. 5th Iranian Conference on Signal Processing and Intelligent Systems (ICSPIS), Semnan, Iran.
Mohammadzaheri;, M., Emadi;, M., Ziaiefar;, H., Ghodsi;, M., Bahadur;, I., Zarog;, M., & Saleem, A. (2019, 23-24 May). *Adaptive Charge Estimation of Piezoelectric Actuators, a Radial Basis Function Approach* 20th International Conference on Research and Education in Mechatronics Wels, Austria
Montgomery, D. C., & Runger, G. (2017). *Probability and Statistics for Engineers*. Wiley.
Nguyen, D., & Widrow, B. (1990, 1990). *Improving the learning speed of 2-layer neural networks by choosing initial values of the adaptive weights* International Joint Conference on Neural Networks, San Diego, USA.
Park, J., & Sandberg, I. W. (1993). Approximation and radial-basis-function networks. *Neural computation*, *5*(2), 305-316.
PiezoDrive. (2021). *Piezoelectric Actuators*. https://www.piezodrive.com/actuators/
Rios, S., & Fleming, A. (2014). Control of Piezoelectric Benders Using a Charge Drive. Proc. Actuator,
Sabek, W., Al-mana, A., Siddiqui, A. R., Assadi, B. E., Mohammad-khorasani, M., Mohammadzaheri, M., & Tafreshi, R. (2015). *Experimental Investigation of Piezoelectric Tube Actuators Dynamics* 2nd International Conference on Robotics and Mechatronics, Madrid, Spain.

Sen, P. C., Hajra, M., & Ghosh, M. (2020). Supervised classification algorithms in machine learning: A survey and review. In *Emerging technology in modelling and graphics* (pp. 99-111). Springer.

Sifaoui, A., Abdelkrim, A., & Benrejeb, M. (2008). On the use of neural network as a universal approximator. *Int. J. Sci. Tech. Control Comput. Eng*, *2*, 386-399.

Singh, K., Sharma, S., Kumar, R., & Talha, M. (2021). Vibration control of cantilever beam using poling tuned piezoelectric actuator. *Mechanics Based Design of Structures and Machines*, 1-24.

Szeremeta, W. K., Harniman, R. L., Bermingham, C. R., & Antognozzi, M. (2021). Towards a Fully Automated Scanning Probe Microscope for Biomedical Applications. *Sensors*, *21*(9), 3027.

Versaci, M., Jannelli, A., Morabito, F. C., & Angiulli, G. (2021). A Semi-Linear Elliptic Model for a Circular Membrane MEMS Device Considering the Effect of the Fringing Field. *Sensors*, *21*(15), 5237.

Xu, Y., Hu, X., Kundu, S., Nag, A., Afsarimanesh, N., Sapra, S., . . . Han, T. (2019). Silicon-based sensors for biomedical applications: a review. *Sensors*, *19*(13), 2908.

Yang, C., Li, C., & Zhao, J. (2017). A Nonlinear Charge Controller With Tunable Precision for Highly Linear Operation of Piezoelectric Stack Actuators. *IEEE Transactions on Industrial Electronics*, *64*(11), 8618-8625.

Yang, X., Li, Z., Fei, C., Liu, Y., Li, D., Hou, S., . . . Zhou, Q. (2020). High frequency needle ultrasonic transducers based on Mn doped piezoelectric single crystal. *Journal of Alloys and Compounds*, *832*, 154951.

Yi, K. A., & Veillette, R. J. (2005). A charge controller for linear operation of a piezoelectric stack actuator. *IEEE Transactions on Control Systems Technology*, *13*(4), 517-526.

Ying, H. (1998). *General Takagi-Sugeno fuzzy systems are universal approximators*. <Go to ISI>://000074668800145

Zhang, X., & Wang, J.-L. (2016). From sparse to dense functional data and beyond. *The Annals of Statistics*, *44*(5), 2281-2321.

Response to Comments and Revision Report

The authors wish to thank the editor and reviewers for their and effort spent on our chapter and their role on improvement of the work. The modifications made in the chapter to address the comments of reviewer 1, 2 and 3 are highlighted in yellow, green and cyan, respectively.

Response to Reviewer 1 Comments

<u>Comment 1</u>-The design of sensors and / or actuators on a micrometric scale is, nowadays, very topical, especially considering the fact that physical-mathematical models are needed that allow real-time recovering of moving parts by means of numerical techniques that can be easily transcribed into hardware. So, I recommend inserting a sentence in the text that highlights this need by putting the following relevant works in the bibliography: doi: 10.3390/s21155237 doi: 10.3390/s19132908 *)

Response: In order to address this comment, a sentence was added to the third paragraph of the introduction including both suggested references.

<u>Comment 2</u>-The caption of Figure 1 deserves a particular study. So I ask that it be made self-explanatory.

Response: The caption of Figure 1 has been expanded to be self-explanatory and to satisfy the reviewer's comment.

<u>Comment 3</u>-After the Introduction the following sentence is reported: "Theoretically, integral of iP is the charge of the actuator. However, such an integration has complications". Please state the reasons.

Response: In fact, the text immediately following the sentence, mentioned by the expert reviewer, aims to explain the reason of integration complications. However, admittedly, there was no clear connection between the sentence and the presented reasons. Therefore, a phrase "The reason is that the" (alongside with a few other amendments) was added to clarify the connection of the aforementioned sentence and its reasons and to address the raised comment.

<u>Comment 4</u>- In the section "PROBLEM STATEMENT" it would be interesting to insert some mathematical details of the modeling to better understand the intrinsic links between the various variables.

Response: Both equations (3) and (4) have been revised and supplied with more details to further clarify their meaning and satisfy the raised comment.

<u>Comment 5</u>- In the Section "ARTIFICIAL INTELLIGENCE APPROACH TO APPROXIMATE THE SENSING RESISTOR" neurofuzzy networks are mentioned as function approximators. It would be interesting to highlight the versatility of these approaches by inserting works transversal to the proposed methodology in the bibliography. In particular, I recommend inserting: doi: 10.1023/A:1020333704205 doi: 10.1016/j.fss.2004.07.001 which represents a family stone in the sizing of microstrip antennas through the use of neurofuzzy techniques.

Response: Both valuable references, recommended by the reviewer, have been used and cited to enrich the subsection of "Neurofuzzy Networks" of the chapter.

Comment 6-In the Tables, please highlight the most relevant numerical results in bold.
Response: Done

Response to Reviewer 2 Comments

Comment 1- In title, “an Artificial Intelligence Approach” is written. Please clearly indicate the Artificial Intelligence Approach.

Response: As mentioned in the last sentence of the abstract, the last sentence of the sixth paragraph of the introduction and the first paragraph of a section entitled “Artificial Intelligence Approach to Approximate the Sensing Resistor”. This book chapter employs five different artificial intelligence techniques to solve the design problem, detailed in “Problem Statement”, instead of analytical modelling. That is, “an Artificial Intelligence Approach” has been used to tackle the stated problem.

Comment 2- “The employed types of models are radial basis function networks, RBfNs (both exact and efficient types), neurofuzzy networks, multi-layer perceptions, MLPs, and fully connected cascade, FFC, networks.” is written. What is the difference of multi-layer perceptions and MLPs?

Response: MLP is the acronym for multi-layer perceptron, as mentioned in the title of a subsection “Multi-layer Perceptrons (MLPs)”. The introduction and the first paragraph of “Artificial Intelligence Approach to Approximate the Sensing Resistor” section have been modified to clarify this matter and to address this comment.

Comment 3- The reviewer wonders that why the authors did not use some suitable, relevant sensors to measure the charge for piezoelectric actuators. How is the charge amplifier or oscilloscope?

Response: In fact, no oscilloscope can measure charge. Furthermore, charge amplifiers (or charge drives) of piezoelectric actuators are actually a combination of a charge estimator and a feedback control system; thus, a charge estimator is needed first to have a charge amplifier. A digital charge estimator with an intuitively chosen sensing resistance, as reported in the literature and discussed in the chapter, may lead to low precision or high voltage drop or very commonly both. An appropriate design of charge estimators for piezoelectric actuators as detailed in sections “Digital Charge Estimators of Piezoelectric Actuators” and “Problem Statement” should maximise the precision, keep the voltage drop low and minimise the effect of drift, a multi-objective complicated design problem investigated for decades by many research groups. This chapter successfully tackles this design problem with use of artificial intelligence techniques.

Comment 4- Suspicious fonts are seen in equations.

Response: The reason of the mentioned fonts was the PDF maker used to prepare in the original version. The PDF maker has now been changed, and the problem is fixed.

Comment 5- The overall contents sounds far from “Handbook of Research on New Investigations in Artificial Life, AI, and Machine Learning”. Detailed description and figures of AI are not included in this manuscript.

Response: In order to address the comment, the authors added Fig.9 to the chapter to depict FFC networks and MLPs . All AI models have been described mathematically in full in the chapter, and Fig.8 depicts the rules of a neurofuzzy network. The chapter demonstrates the use of Artificial Intelligence (AI) techniques to solve a complex engineering design problem, and shows the superiority of AI over analytical approach; such a topic seems to fit well into the handbook,

Response to Reviewer 3 Comments

Comment 1- The author(s) provide enough numbers of references in the chapter. However, the chapter does not provide sufficient background information and literature review for artificial intelligence in the introduction part. The chapter's main topic is artificial intelligence; therefore, the author(s) must enhance the introduction part for artificial intelligence. Also, there are no allied studies about parameter estimation methods using artificial intelligence. The author(s) should review the parameter estimation method using artificial intelligence in the introduction part.

Response: Two paragraphs have been added to the end of the introduction concerning with the employed AI methods to address the reviewer's comment. Only two new references were cited in these paragraphs (along with some existing references) to avoid having excessive number of references for the chapter.

Comment 2- There is no explanation for why the author(s) hired the specific five artificial intelligence.

Response: a paragraph, newly added to the introduction, provides the explanation mentioned by the reviewer: "As detailed in "Problem Statement", the chapter particularly requires AI techniques to identify a mathematical function out of experimental input-output data. Data-driven system modelling (or regression) methods based on supervised learning suit such a purpose (Sen et al., 2020). To the best of authors' knowledge, only five AI methods in this category are universal approximators, with verified ability for data-driven modelling (Chen & Chen, 1995; Mohammadzaheri et al., 2012; Mohammadzaheri et al., 2018; Park & Sandberg, 1993; Ying, 1998). All these methods are examined in this chapter to tackle the stated problem, and their performance is compared.

Comment 3- Also, there is no description of how the author(s) implements artificial intelligence to approximate the sensing resistor. Does the author(s) use C language or MATLAB?

Response: The description, mentioned by the reviewer, has been added to the end of the first paragraph of "Artificial Intelligence Approach to Approximate the Sensing Resistor" section to address this comment: "The models were developed through programming in MATLAB 9.4 with occasional use of commands from Neural Network Toolbox Version 11.1 and Fuzzy Logic Toolbox Version 2.3.1 of the software package".

Comment 4- It isn't easy to follow each artificial intelligence only by reading the sections. Would you please enhance each section so that the reader can do follow-up experiments using this chapter?

Response: All subsections of "Artificial Intelligence Approach to Approximate the Sensing Resistor" section have been revised to improve their readability and to address this comment. However, the reviewer is requested to kindly consider that full coverage of all these methods in a section of a book chapter is almost impossible. The authors have tried to present the techniques as concise as they could. However, the authors had to refer the readers to other publication in topics such as MLP's parameter initialisation and identification .All these techniques perhaps need a full textbook to provide the reader with full understanding and ability to develop the models. By the way, all parameters that one needs to re-develop the models have been provided to the readers. These include the range and the increment of spread and target error in RBFNs, influence range, squash factor, accept ratio and reject ratio used in subtractive clustering to find initial fuzzy models, number of layers/neurons and their activation functions in MLPs and FFCs, as well as details or at least the title of parameter initialisation and identification algorithms with references. Therefore, a reader with adequate familiarity with the models can repeat the process with some efforts. The authors are willing to share their raw data with the publisher or alternatively, make them freely available on researchgate for interested researchers.

Comment 5- The reviewer could not understand the novelty and usefulness of this chapter. Commentary on the novelty and usefulness of this chapter should be added.

Response: In order to address the comment, extra explanations were added to the chapter. As an instance, the following explanations were added to the conclusion: "Accurate identification of the formula, mentioned in the previous paragraph, leads to development of highly charge/position estimators with slight voltage drop. Such estimators can replace bulky and expensive position sensors and open new horizons to nanopositioning. Analytical models have already failed to accurately identify the aforementioned formula".

Generally speaking, useful sensors in piezo actuated (and other types of) nanopositioning are expensive and rather difficult to run/calibrate, More importantly, they need considerable space that may not be available at all, e.g. in highly accurate surgeries. Charge/position estimation methods can replace these sensors, but they may take a large portion of the voltage applied to the actuators. Finding an accurate charge/position estimator, which takes a small voltage, can be a breakthrough and opens the door to new applications of nanopositioning. Formulation of charge/position design problem clarifies the need for identification of functions in equation 4 of the chapter to design appropriate charge estimators. Analytical methods have failed to serve this purpose. This chapter shows AI techniques can handle this task very well, and MLP is the best of them to tackle the task.

Comment 6- There is no discussion about why the MLP is suitable to solve the approximate sensing resistor. Also, why the other artificial intelligence is not good to solve the problems?

Response: The following discussion was added to the section "Results and Discussions" to justify superior performance of the MLPs: "The MLPs have the smallest number of parameters amongst the models, 21, while they still fully meet the requirements of Kolmogorov's theorem. Relatively low number of parameters can play a major role in their performance, considering the fact that the modelling data could be as small as 25 data sets". It should be noted that other presented AI techniques are fairly good in charge estimation, e.g. if their results are compared with the results of analytical model ,e.g. in (Mohammadzaheri et al., 2019). They are just not as good as the MLP.

References for Response to Comments

Chen, T. P., & Chen, H. (1995). Approximation capability to functions of several variables, nonlinear functionals, and operators by radial basis function neural networks. *IEEE Transactions on Neural Networks*, *6*(4), 904-910. <Go to ISI>://A1995RF58200008

Mohammadzaheri, M., Chen, L., & Grainger, S. (2012). A critical review of the most popular types of neuro control. *Asian Journal of Control*, *16*(1), 1-11.

Mohammadzaheri, M., Emadi, M., Ghodsi, M., Jamshidi, E., Bahadur, I., Saleem, A., & Zarog, M. (2019). A variable-resistance digital charge estimator for piezoelectric actuators: An alternative to maximise accuracy and curb voltage drop. *Journal of Intelligent Material Systems and Structures*, *30*(11), 1699-1705.

Mohammadzaheri, M., Ghodsi, M., & AlQallaf, A. (2018). Estimate of the Head Produced by Electrical Submersible Pumps on Gaseous Petroleum Fluids, a Radial Basis Function Network Approach. *International Journal of Artificial Intelligence Applications*, *9*(1).

Park, J., & Sandberg, I. W. (1993). Approximation and radial-basis-function networks. *Neural computation*, *5*(2), 305-316.

Sen, P. C., Hajra, M., & Ghosh, M. (2020). Supervised classification algorithms in machine learning: A survey and review. In *Emerging technology in modelling and graphics* (pp. 99-111). Springer.

Ying, H. (1998). *General Takagi-Sugeno fuzzy systems are universal approximators*. <Go to ISI>://000074668800145